Peer reviewed version

University of Bristol - Explore Bristol Research
General rights

Atomically-engineered epitaxial anatase TiO₂ metal-semiconductor field-effect transistors

Brian S. Y. Kim,[1,2,a)] Makoto Minohara,[3,4] Yasuyuki Hikita,[3] Christopher Bell,[3,5] Harold Y. Hwang[2,3,a)]

[1] *Department of Electrical Engineering, Stanford University, Stanford, California 94305, USA*

[2] *Geballe Laboratory for Advanced Materials, Department of Applied Physics, Stanford University, Stanford, California 94305, USA*

[3] *Stanford Institute for Materials and Energy Sciences, SLAC National Accelerator Laboratory, Menlo Park, California 94025, USA*

[4] *Photon Factory, Institute of Materials Structure Science (IMSS), High Energy Accelerator Research Organization (KEK), Tsukuba, Ibaraki 305-0801, Japan*

[5] *School of Physics, University of Bristol, Tyndall Avenue, Bristol BS8 1TL, United Kingdom*

Anatase TiO₂ is a promising material for a vast array of electronic, energy, and environmental applications, including photocatalysis, photovoltaics, and sensors. A key requirement for these applications is the ability to modulate its electrical properties without dominant dopant scattering and while maintaining high carrier mobility. Here we demonstrate the room temperature field-effect modulation of the conducting epitaxial interface between anatase TiO₂ and LaAlO₃ (001), which arises for LaO-terminated LaAlO₃, while the AlO₂-terminated interface is insulating. This approach, together with the metal-semiconductor field-effect transistor geometry, naturally bypasses the gate/channel interface traps, resulting in a high field-effect mobility μ_{FE} of 3.14 cm² (V s)⁻¹ approaching 98% of the corresponding Hall mobility μ_{Hall}. Accordingly, the channel conductivity is modulated over 6 orders of magnitude over a gate voltage range of ~4 V.

a)Authors to whom the correspondence should be addressed. Electronic mail: bkim0825@stanford.edu.

Applications based on the multifunctional properties of anatase TiO_2, including ferromagnetism,[1,2] transparent conductivity,[3,4] and diverse photocatalytic effects,[5–8] are often limited by a low carrier mobility, arising especially from the effects of the bulk dopants. For example, dopants in photoelectrochemical (PEC) cells adversely affect the PEC activity by acting as recombination sites for photoexcited carriers.[9] Furthermore, the sensitivity of TiO_2-based gas sensors can dramatically decrease with a reduced carrier mobility.[10–13] In this regard, the ability to modulate the intrinsic properties of anatase TiO_2 without bulk dopants can be a promising pathway to overcome these limitations. For example, an epitaxial strain can be used to engineer the facet orientation and crystal structure of TiO_2 for enhanced photocatalytic activity.[14,15] Another key example is to tune the carrier density using external fields, which can induce ferromagnetism,[2] and amphiphilic[7] or superhydrophobic[16] surfaces in TiO_2. More specifically, electrically tuning the carrier density using a metal-semiconductor field-effect transistor (MESFET) geometry[17] has a natural advantage for our purposes. The carrier mobility can be significantly improved since the band-bending pushes the carriers away from the gate/channel interface traps and defects,[17,18] as distinct from the conventional metal-oxide-semiconductor field-effect transistor (MOSFET) geometry.[19–21]

Using this approach, here we demonstrate conductivity modulation of epitaxial anatase TiO_2 using the MESFET geometry at room temperature. We adopt the recently reported technique[22,23] of atomistically changing the boundary conditions of the anatase TiO_2/$LaAlO_3$ (001) heterointerface to introduce the carriers to the channel. Analogous to modulation doping,[24] this approach circumvents dopant and crystal defects present in bulk chemical doping and was shown to achieve high carrier mobilities in an interface specific manner.[22] This heterostructure was fabricated using pulsed laser deposition (see supplementary material) by first changing the surface termination layer of the $LaAlO_3$ (001) substrate from AlO_2 to LaO, followed by the

deposition of ~24 nm thick (001)-oriented anatase TiO_2 (Figure 1(a) and 1(b)). Single-crystalline growth of the heterostructure is evident from the atomically flat surface morphology with root mean square roughness below ~0.3 nm as seen by atomic force microscopy (AFM), and the clear (4 × 1) surface-reconstructed reflection high-energy electron diffraction (RHEED) patterns (Figure 1(c) and 1(d)). X-ray diffraction (XRD) measurements further confirm single-crystalline growth. A clear $LaAlO_3$ (002) substrate peak and an anatase TiO_2 (004) peak are observed, but no other peaks are present above the noise level (Figure 2(a)). These measurements indicate the high quality epitaxial growth of (001)-oriented anatase TiO_2 thin films.[19–21,25]

We first developed and demonstrate successful device isolation using a pre-deposited amorphous AlO_x hard mask, as evident from the Raman spectroscopy (532 nm wavelength) performed on our devices (Figure 2(b)). Clear anatase peaks[26] corresponding to the B_{1g} (399 cm^{-1}), a doublet of A_{1g} and B_{1g} (516 cm^{-1}), and E_g (639 cm^{-1}) modes were observed in the channel region. In contrast, rutile peaks[27] corresponding to the E_g (446 cm^{-1}) and A_{1g} (611 cm^{-1}) modes superimposed on a large background signal were found in the areas covered by the hard mask. The broad mid-intensity peak around ~260 cm^{-1} from the hard mask corresponds to two-phonon scattering.[27] This emergence of rutile peaks emphasizes the importance of the epitaxial stabilization provided by the atomically flat single-crystalline $LaAlO_3$ (001) substrate to artificially induce crystalline anatase TiO_2 growth. TiO_2 grown on top of the hard mask formed in the thermodynamically more stable rutile phase,[28] showing a large background signal due to amorphous TiO_x formation. The current flow measured across TiO_2 grown on top of the hard mask was below the noise level of the measurement setup (<10 fA at 1.5 V). The amorphous AlO_x hard mask therefore serves as a robust device isolation method.

On these isolated crystalline anatase regions, a Pt gate was further deposited. The Pt/anatase TiO_2 gate current–voltage (*I–V*) characteristics show clear Schottky diode behavior with I_G

increasing exponentially in the forward-bias regime (Figure 3(a)). The saturation of I_G at higher V_{GS} is due to the series resistance of the anatase TiO_2 thin film. Using a thermionic emission model and an electron effective mass m^* of ~1.3 m_0[21,29] (where m_0 is the free electron mass), the extracted mean Schottky barrier height $\overline{\phi_{SB}}$ and mean ideality factor $\overline{\eta}$ are 1.20 ± 0.16 eV and 1.28 ± 0.16, respectively. The reverse-bias leakage current was also successfully suppressed down to the picoamp order, which is essential for the MESFET because it operates in the reverse-bias regime, i.e. $V_{GS} < 0$ V.

Using these device structures, MESFET operation is observed from the clear transconductance of the output characteristics I_D–V_{DS} with applied V_{GS} ranging from 0 V to −7 V, in 0.5 V steps (Figure 3(b)). We observe the pinch-off and current saturation behavior expected for an ideal MESFET. Channel depletion is also evident from the decrease in the saturation current when a negative V_{GS} is applied. Furthermore, the linear dependence of $\sqrt{I_D}$ with a small V_{GS} in the saturation regime at $V_{DS} = 5$ V is consistent with the expected quadratic approximation (Figure 3(c)).[17] The mean threshold voltage $\overline{V_{Th}}$ deduced from the abscissa of the linear fit to $\sqrt{I_D}$–V_{GS} is −2.53 ± 0.24 V. Notably, one key advantage of using the Schottky gate is that the channel conductivity can be tuned effectively using the orders of magnitude larger internal electric field compared to that externally generated in the MOSFET structure with the same applied bias.[30] As a result, the on/off current ratio can exceed 10^6 within a gate voltage range of ~4 V (Figure 3(d)), which is substantially smaller than ~20 V to ~100 V required in previously reported MOSFET geometry based on epitaxial anatase TiO_2 to fully turn the devices on and off.[19–21] A significantly smaller operating voltage combined with high reproducibility would further enable transistor circuits[31] incorporating anatase TiO_2. Note that hysteresis between the forward and reverse V_{GS} sweeps is negligible, illustrating minimal effects from the gate/channel interface traps on the modulation and conductivity of the channel.

4

The field-effect mobility μ_{FE} of the MESFET is extracted in the saturation regime at $V_{DS} = 5$ V

from the following equation for the transconductance g_m:[17]

$$g_m = \partial I_D / \partial V_{GS} = (e\mu_{FE} N_{2D} W_G / L_G)\{1 - [(V_{bi} - V_{GS})/(V_{bi} - V_{Th})]^{1/2}\} \qquad (1)$$

where e is the elementary charge, N_{2D} is the sheet carrier density, W_G is the gate width, L_G is the

gate length, and V_{bi} is the built-in potential of the Schottky gate. $N_{2D} = 2.42 \times 10^{13}$ cm^{-2} is

extracted from Hall measurements performed on the ungated channel of the device (Figure 4(a)).

$V_{bi} = 1.17$ eV is extracted using the full depletion approximation, $V_{bi} = \phi_{SB} + (E_F - E_C)$, where

E_C is the conduction band edge and E_F is the Fermi level. Here we assume a non-degenerate

semiconductor with the effective density of states N_C in the conduction band of $2(2\pi m^* k_B T/h^2)^{3/2}$,

where k_B is the Boltzmann constant, T is the operating temperature, and h is the Planck constant.

This is consistent with the observed activated form of the temperature dependence of the

resistivity for TiO$_2$ structures of this thickness. For a more precise derivation of μ_{FE}, the effective

gate voltage V'_{GS} incorporating the voltage drop across the ungated source is used:[32] $V'_{GS} =$

$V_{GS} - I_D R_S$, where $R_S = 153.73$ kΩ is the four-probe resistance of the ungated channel, which

results in a voltage drop of $I_D R_S \sim 0.9$ V.

Figure 4(b) shows the $\mu_{FE} - V_{GS}$ characteristics of the MESFET. μ_{FE} continuously increases as

V_{GS} tends to 0 V, and a maximum μ_{FE} of 3.14 cm^2 (V s)$^{-1}$ is achieved at $V_{GS} = 0$ V, which is

significantly higher than ~0.04 cm^2 (V s)$^{-1}$ to ~0.9 cm^2 (V s)$^{-1}$ previously obtained in the

MOSFET geometry.[19–21] Note that the corresponding Hall mobility μ_{Hall} of our devices is 3.20

cm^2 (V s)$^{-1}$, which is smaller compared to the value of 25 cm^2 (V s)$^{-1}$ observed for thicker films

in the previous report.[22] Thus μ_{FE} of our devices can be enhanced by using a thicker channel, but

as a tradeoff requiring higher gate voltages for operation. Furthermore, μ_{FE} reaches 98% of μ_{Hall},

which is again striking compared to ~13% in the MOSFET geometry.[21] This illustrates the

intrinsic advantage of both the MESFET geometry and the absence of conventional bulk chemical dopants in the channel. In particular, μ_{Hall} corresponds to the itinerant carrier mobility because the Hall signal does not probe localized states, whereas μ_{FE} can be significantly affected by carriers localized in the channel.[33] Therefore, the minimal underestimation of μ_{FE} compared to μ_{Hall} still present in our devices can be interpreted in terms of the carrier localization at intrinsic defect sites of the anatase TiO_2 thin film, such as remnant oxygen vacancies[34] or naturally arising antiphase grain boundaries[22,35] due to the existence of the two equally probable epitaxial relationships between anatase TiO_2 and $LaAlO_3$ (001) substrate.

In conclusion, we show that the conductivity of epitaxial anatase TiO_2 induced by atomistically controlling the anatase $TiO_2/LaAlO_3$ (001) interface boundary conditions can be effectively modulated in the Schottky gate geometry. The field-effect mobility μ_{FE} reaches as high as 3.14 cm^2 (V s)$^{-1}$, approaching 98% of the corresponding Hall mobility μ_{Hall}, and the channel conductivity can be modulated over 6 orders of magnitude with a small gate voltage range of ~4 V. This work offers promise for integrating the diverse functionalities of anatase TiO_2 in a wide range of heterostructures and device architectures.

SUPPLEMENTARY MATERIAL

See supplementary material for growth, device fabrication, and characterization.

REFERENCES

[1] Y. Matsumoto, M. Murakami, T. Shono, T. Hasegawa, T. Fukumura, M. Kawasaki, P. Ahmet, T. Chikyow, S. Koshihara, and H. Koinuma, Science 291, 854 (2001).

[2] Y. Yamada, K. Ueno, T. Fukumura, H. T. Yuan, H. Shimotani, Y. Iwasa, L. Gu, S. Tsukimoto, Y. Ikuhara, and M. Kawasaki, Science 332, 1065 (2011).

[3] Y. Furubayashi, T. Hitosugi, Y. Yamamoto, K. Inaba, G. Kinoda, Y. Hirose, T. Shimada, and T. Hasegawa, Appl. Phys. Lett. 86, 252101 (2005).

[4] T. Hitosugi, Y. Furubayashi, A. Ueda, K. Itabashi, K. Inaba, Y. Hirose, G. Kinoda, Y. Yamamoto, T. Shimada, and T. Hasegawa, Jpn. J. Appl. Phys. 44, L1063 (2005).

[5] A. Fujishima and K. Honda, Nature 238, 37 (1972).

[6] A. Sclafani and J. M. Herrmann, J. Phys. Chem. 100, 13655 (1996).

[7] R. Wang, K. Hashimoto, A. Fujishima, M. Chikuni, E. Kojima, A. Kitamura, M. Shimohigoshi, and T. Watanabe, Nature 388, 431 (1997).

[8] M. Grätzel, Nature 414, 338 (2001).

[9] N. Serpone, D. Lawless, J. Disdier, and J.-M. Herrmann, Langmuir 10, 643 (1994).

[10] T. Seiyama and S. Kagawa, Anal. Chem. 38, 1069 (1966).

[11] N. Yamamoto, S. Tonomura, T. Matsuoka, and H. Tsubomura, Surf. Sci. 92, 400 (1980).

[12] J. Bai and B. Zhou, Chem Rev. 114, 10131 (2014).

[13] S. Cui, H. Pu, S. A. Wells, Z. Wen, S. Mao, J. Chang, M. C. Hersam, and J. Chen, Nature Commun. 6, 8632 (2015).

[14] H. G. Yang, C. H. Sun, S. Z. Qiao, J. Zou, G. Liu, S. C. Smith, H. M. Cheng, and G. Q. Lu, Nature 453, 638 (2008).

[15]D. O. Scanlon, C. W. Dunnill, J. Buckeridge, S. A. Shevlin, A. J. Logsdail, S. M. Woodley, C. R. A. Catlow, M. J. Powell, R. G. Palgrave, I. P. Parkin, G. W. Watson, T. W. Keal, P. Sherwood, A. Walsh, and A. A. Sokol, Nature Mater. 12, 798 (2013).

[16]X. Zhang, M. Jin, Z. Liu, D. A. Tryk, S. Nishimoto, T. Murakami, and A. Fujishima, J. Phys. Chem. C 111, 14521 (2007).

[17]S. M. Sze and K. K. Ng, *Physics of Semiconductor Devices* (Wiley, New York, 2007).

[18]K. Hirakawa, H. Sakaki, and J. Yoshino, Phys. Rev. Lett. 54, 1279 (1985).

[19]M. Katayama, H. Koinuma, and Y. Matsumoto, Mater. Sci. Eng. B 148, 19 (2008).

[20]M. Katayama, S. Ikesaka, J. Kuwano, H. Koinuma, and Y. Matsumoto, Appl. Phys. Lett. 92, 132107 (2008).

[21]Y. Nagao, A. Yoshikawa, K. Koumoto, T. Kato, Y. Ikuhara, and H. Ohta, Appl. Phys. Lett. 97, 172112 (2010).

[22]M. Minohara, T. Tachikawa, Y. Nakanishi, Y. Hikita, L. F. Kourkoutis, J.-S. Lee, C.-C. Kao, M. Yoshita, H. Akiyama, C. Bell, and H. Y. Hwang, Nano Lett. 14, 6743 (2014).

[23]J. Cheng, J. Luo, and K. Yang, ACS Appl. Mater. Interfaces 9, 7682 (2017).

[24]R. Dingle, H. L. Störmer, A. C. Gossard, and W. Wiegmann, Appl. Phys. Lett. 33, 665 (1978).

[25]M. Murakami, Y. Matsumoto, K. Nakajima, T. Makino, Y. Segawa, T. Chikyow, P. Ahmet, M. Kawasaki, and H. Koinuma, Appl. Phys. Lett. 78, 2664 (2001).

[26]T. Ohsaka, F. Izumi, and Y. Fujiki, J. Raman Spectrosc. 7, 321 (1978).

[27]S. P. S. Porto, P. A. Fleury, and T. C. Damen, Phys. Rev. 154, 522 (1967).

[28]D. A. H. Hanaor and C. C. Sorrell, J. Mater. Sci. 46, 855 (2011).

[29]H. Tang, K. Prasad, R. Sanjinès, P. E. Schmid, and F. Lévy, J. Appl. Phys. 75, 2042 (1994).

[30]T. Yajima, Y. Hikita, and H. Y. Hwang, Nature Mater. 10, 198 (2011).

[31]W. I. Park, J. S. Kim, G.-C. Yi, and H.-J. Lee, Adv. Mater. 17, 1393 (2005).

[32]S. A. Fortuna and X. Li, IEEE Electron Device Lett. 30, 593 (2009).

[33]V. Podzorov, E. Menard, J. A. Rogers, and M. E. Gershenson, Phys. Rev. Lett. 95, 226601 (2005).

[34]T. Tachikawa, M. Minohara, Y. Nakanishi, Y. Hikita, M. Yoshita, H. Akiyama, C. Bell, and H. Y. Hwang, Appl. Phys. Lett. 101, 022104 (2012).

[35]S. Zheng, C. A. J. Fisher, T. Kato, Y. Nagao, H. Ohta, and Y. Ikuhara, Appl. Phys. Lett. 101, 191602 (2012).
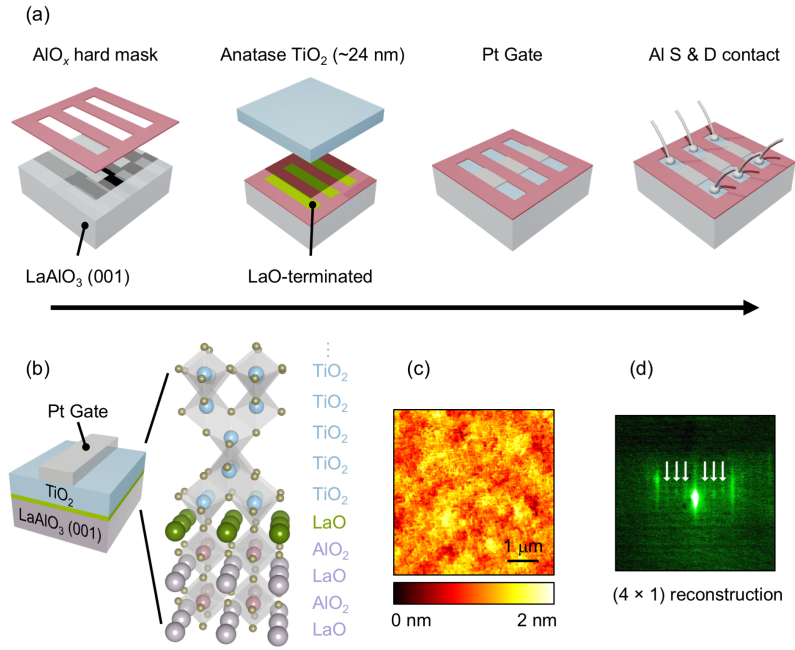
FIG. 1. Room-temperature MESFET device (a) process flow and (b) schematics. 1 u.c. deposition of La_2O_3 target flips the surface termination of $LaAlO_3$ (001) substrate from AlO_2 to LaO, which changes the anatase $TiO_2/LaAlO_3$ (001) interface boundary conditions. Subsequently deposited ~24 nm anatase TiO_2 is used as the active channel of the device, with dimensions of 1.2 mm × 0.29 mm, and a Pt/anatase TiO_2 Schottky gate is used. (c) AFM surface morphology of the anatase TiO_2 (scan area 5 μm × 5 μm). (d) (4 × 1) surface-reconstructed RHEED patterns of the (001)-oriented anatase TiO_2. Arrows show the additional streaks arising from surface reconstruction.
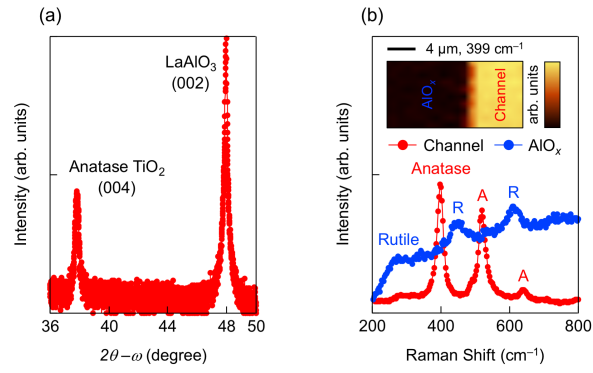
FIG. 2. (a) XRD patterns of the MESFET before Pt Schottky gate deposition showing a $LaAlO_3$ (002) substrate peak and anatase TiO_2 (004) peak. (b) Raman scattering intensity verses Raman shift with clear anatase peaks corresponding to the B_{1g} (399 cm^{-1}), a doublet of A_{1g} and B_{1g} (516 cm^{-1}), and E_g (639 cm^{-1}) modes from the channel region (red closed circles). On the amorphous AlO_x hard mask, rutile peaks corresponding to the E_g (446 cm^{-1}) and A_{1g} (611 cm^{-1}) modes superimposed on a large background signal due to the amorphous TiO_x were observed (blue closed circles). Note that the broad mid-intensity peak around ~260 cm^{-1} from the hard mask corresponds to two-phonon scattering. The inset shows the Raman intensity map of the corresponding device at the B_{1g} mode of anatase TiO_2 (399 cm^{-1}), confirming that anatase TiO_2 only forms on the exposed channel.
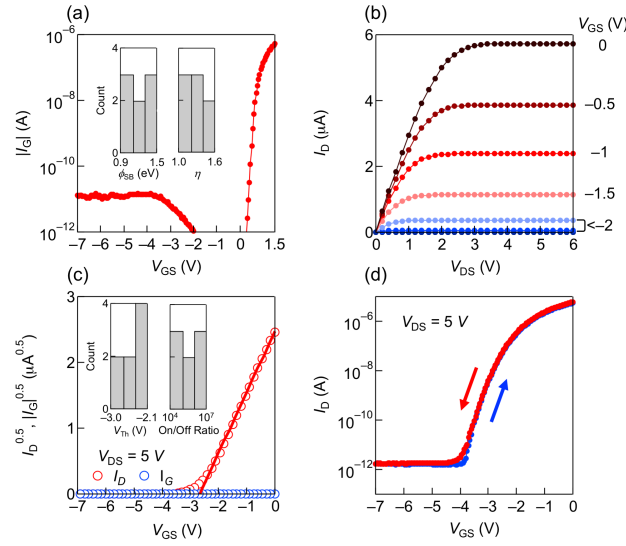
FIG. 3. Room-temperature device characteristics of the MESFET. (a) I–V characteristics of the Pt/anatase TiO$_2$ Schottky diode forming the FET gate. For eight MESFETs characterized, the mean Schottky barrier height $\overline{\phi_{SB}}$ is 1.20 ± 0.16 eV, and the mean ideality factor $\overline{\eta}$ is 1.28 ± 0.16. The inset shows histograms for ϕ_{SB} and η. (b) I_D–V_{DS} output characteristics with a clear pinch-off and current saturation behavior. (c) $\sqrt{I_D}$–V_{GS} transfer characteristics in the saturation regime at $V_{DS} = 5$ V showing linear behavior. The mean threshold voltage $\overline{V_{Th}} = -2.53 \pm 0.24$ V is deduced from the abscissa of the linear fit. The inset shows histograms for V_{Th} and the on/off current ratio. (d) I_D–V_{GS} transfer characteristics plotted on a semi-logarithmic scale, showing that the on/off current ratio can exceed 10^6. The arrows indicate the sweep direction of V_{GS}. A gate voltage range of ~4 V can fully turn the devices on and off.
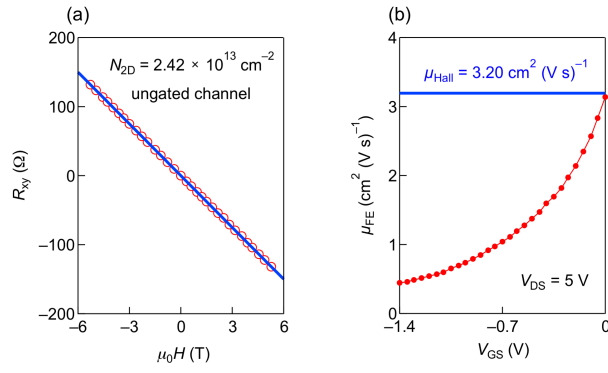
FIG. 4. (a) R_{xy} verses $\mu_0 H$ of the ungated channel of the MESFET at room temperature (red open circles), and the linear fit (blue solid) used to extract the sheet carrier density $N_{2D} = 2.42 \times 10^{13}$ cm^{-2}. (b) Room-temperature μ_{FE}–V_{GS} characteristics (red closed circles) in the saturation regime at $V_{DS} = 5$ V. The blue solid line corresponds to μ_{Hall} of the ungated channel of the same device.